

Spin susceptibility for orbital-singlet Cooper pair in the three-dimensional Sr₂RuO₄ superconductor

Yuri Fukaya,^{1,2} Tatsuki Hashimoto,^{1,3} Masatoshi Sato,¹ Yukio Tanaka,⁴ and Keiji Yada⁴

¹*Yukawa Institute for Theoretical Physics, Kyoto University, Kyoto 606-8502, Japan*

²*CNR-SPIN, I-84084 Fisciano (Salerno), Italy, c/o Università di Salerno, I-84084 Fisciano (Salerno), Italy*

³*Department of Mechanical Engineering, Stanford University, Stanford 94305, California, USA*

⁴*Department of Applied Physics, Nagoya University, Nagoya 464-8603, Japan*

We study the spin susceptibility of the orbital-singlet pairings, including the spin-triplet/orbital-singlet/*s*-wave E_g representation proposed by Suh *et al.*, [H. G. Suh *et al.*, Phys. Rev. Research **2**, 032023 (2020)], for a three-orbital model of superconducting Sr₂RuO₄ in three dimensions. For the pseudospin-singlet states represented in the band basis, the spin susceptibility decreases when reducing the temperature, irrespective of the direction of the applied magnetic fields, even if they are spin-triplet/orbital-singlet pairings in the spin-orbital space. However, because the pseudospin-triplet \mathbf{d} -vector in the band basis is not completely aligned in the xy -plane (along z -axis) owing to the strong atomic spin-orbit coupling, the spin susceptibility for spin-singlet/orbital-singlet/odd-parity pairings is reduced around 5-10 percent with the decrease of the temperature along the z (x) axis. We can determine the symmetry of the pseudospin structure of the Cooper pair by the temperature dependence of the spin susceptibility measured by nuclear magnetic resonance experiments. Our obtained results serve as a guide to determine the pairing symmetry of Sr₂RuO₄.

I. INTRODUCTION

Pairing symmetry in the Sr₂RuO₄ (SRO) superconductor (SC) [1–3] has been an unresolved issue in condensed matter physics. Based on the previous various experiments, e.g., polarized neutron scatterings [4], half-quantum vortices [5, 6], charge transport properties in junctions [7–14], and the nuclear-magnetic-resonance (NMR) measurements [15], spin-triplet/chiral p -wave pairing with time-reversal symmetry (TRS) breaking [$(p_x + ip_y)$ -wave pairing] [16] has been believed to be the most promising one. In addition, theoretical studies also supported the realization of spin-triplet/ p -wave pairing [17–30]. However, recent NMR experiments, that solved the heating issues of the sample in the actual measurement process reported the reduction of the spin susceptibility with the in-plane magnetic field [31–33] below T_c . These experiments seem to be inconsistent with spin-triplet/chiral p -wave where the \mathbf{d} -vector is aligned along the c -axis of SRO [34].

Experimental signatures of a two-component superconducting order parameter in SRO were observed in ultrasound and thermodynamics experiments [35–37]. Several theoretical studies focused on the two-component order parameter with TRS breaking: the accidentally degenerate pairing [$(s' + d_{x^2-y^2})$ -wave [38], $d_{x^2-y^2} + ig_{xy(x^2-y^2)}$ -wave [39–42], and $(s + id_{xy})$ -wave [43, 44]], and the interorbital $d_{zx} + id_{yz}$ -like spin-triplet/orbital-singlet/ s -wave E_g pairing [45] with the Bogoliubov Fermi surface [46, 47]. In the last case, the presence of the t_{2g} -orbital degrees of freedom and strong atomic spin-orbit coupling in SRO [45, 48–50] can generate the orbital-singlet state. The pairing mechanism of the spin-triplet/orbital-singlet/ s -wave pairing is due to the attractive channel $U' - J < 0$ with the interorbital repulsive interaction U' and the renormalized Hund's coupling

J [45, 48]. In addition, the recent experiment under hydrostatic pressure and disorder indicated the $d_{zx} + id_{yz}$ -wave state [51].

To determine the spin structure of the Cooper pair, the temperature dependence of the spin susceptibility in the NMR experiments gives us the important information [15, 31–33]. In the theoretical approaches in SRO, spin susceptibility was calculated in the spin-triplet/orbital-singlet/ s -wave pairing with the \mathbf{d} -vector along the z -axis as a function of the temperature [52] and under the uniaxial strain [53] in the two-dimensional multi-orbital SRO model. Since there are three t_{2g} -orbitals near the Fermi level in SRO, it is necessary to study the temperature dependence of the spin susceptibility for the possible orbital-singlet Cooper pair taking into account the orbital nature. Then, we must adopt the “three-dimensional” SRO Hamiltonian to investigate the orbital-singlet $d_{zx} + id_{yz}$ -like pair potential [45].

In this paper, we calculate the temperature dependence of the spin susceptibility below the critical temperature T_c for orbital-singlet pairings in the three-dimensional SRO model by choosing the possible irreducible representations. We focus on the spin-triplet/orbital-singlet/ s -wave and spin-singlet/orbital-singlet/odd-parity pairings stemming from the multi-orbital and strong atomic spin-orbit coupling. In the first case, the pseudospin-singlet pairing is realized in the band basis, then the resulting spin susceptibility is reduced with the decrease of temperature irrespective of the direction of the magnetic field for all possible irreducible representations. In the second case, the spin susceptibility changes around 5% (10%) by the temperature along the x (z) axis, because the pseudospin-triplet \mathbf{d} -vector in the band basis is not perfectly aligned in the xy -plane (z -axis) away from the xy -symmetric plane owing to the strong atomic spin-orbit coupling. We conclude that the recently observed spin susceptibility of NMR ex-

periments in SRO [31–33] can be explained by the spin-triplet/orbital-singlet/*s*-wave E_g representation.

II. MODEL HAMILTONIAN AND FORMULATION

In this section, we show the model Hamiltonian and the formulation to calculate the spin susceptibility in SRO.

SRO has the $I4/mmm$ tetragonal space group with the point group D_{4h} [2]. The conduction bands of SRO mainly consist of t_{2g} -orbitals [d_{yz} , d_{zx} , and d_{xy}] in the Ru ions. The Hamiltonian in SRO is written as

$$\hat{H} = \sum_{\mathbf{k}} \hat{C}_{\mathbf{k}}^\dagger \hat{H}(\mathbf{k}) \hat{C}_{\mathbf{k}}, \quad (1)$$

where $\hat{C}_{\mathbf{k}}^\dagger = [c_{yz,\uparrow\mathbf{k}}^\dagger, c_{zx,\uparrow\mathbf{k}}^\dagger, c_{xy,\uparrow\mathbf{k}}^\dagger, c_{yz,\downarrow\mathbf{k}}^\dagger, c_{zx,\downarrow\mathbf{k}}^\dagger, c_{xy,\downarrow\mathbf{k}}^\dagger]$ is the creation operator of electrons in t_{2g} -orbitals. For \hat{H} in Eq. (1), we adopt the three-dimensional Hamiltonian in Refs. [43, 45, 49, 54–58],

$$\hat{H}(\mathbf{k}) = \sum_{l,j} h_{lj}(\mathbf{k}) \hat{\Lambda}_l \otimes \hat{\sigma}_j, \quad (2)$$

where $\hat{\Lambda}_{l=0\sim 8}$ are the Gell-Mann matrices as shown in Appendix A, and $\hat{\sigma}_{j=0,x,y,z}$ are the Pauli ones in the spin space. [The explicit form of $h_{lj}(\mathbf{k})$ is given in Appendix A.]

In the superconducting state, the Bogoliubov–de Gennes (BdG) Hamiltonian is given by

$$\hat{H}_{\text{BdG}}(\mathbf{k}) = \begin{pmatrix} \hat{H}(\mathbf{k}) & \hat{\Delta}(\mathbf{k}) \\ \hat{\Delta}^\dagger(\mathbf{k}) & -\hat{H}^*(-\mathbf{k}) \end{pmatrix}, \quad (3)$$

with the pair potential (energy gap function) $\hat{\Delta}(\mathbf{k})$. Here, we consider the pair potential by the symmetry of the Cooper pair. The present model Hamiltonian has the parity dependence in \mathbf{k} and spin-orbital degrees of freedom. Then the pair potential can classify the four types of Cooper pair that satisfy the Fermi-Dirac statistics: spin-singlet/orbital-triplet/even-parity (STE), spin-triplet/orbital-triplet/odd-parity (TTO), spin-triplet/orbital-singlet/even-parity (TSE), and spin-singlet/orbital-singlet/odd-parity (SSO). In our study, we focus on the orbital-singlet pair potentials, i.e., TSE and SSO. Note that we do not consider the odd-frequency pairing in the pair potential because we do not adopt the retardation effect in the attractive channel [59–63]. For TSE states, we assume the “*isotropic*” pairing and the energy gap function is independent of \mathbf{k} . The TSE states are described by the spin-triplet potentials [45, 48, 49, 58],

$$\hat{\Delta} = \Delta(T) [\hat{L}_i \otimes \hat{\sigma}_j] i\hat{\sigma}_y, \quad (4)$$

with $i, j = x, y, z$ and the t_{2g} -orbital angular momentum operators projected onto $L = 2$ in the [d_{yz} , d_{zx} , d_{xy}] basis,

$$\hat{L}_x = \begin{pmatrix} 0 & 0 & 0 \\ 0 & 0 & i \\ 0 & -i & 0 \end{pmatrix}, \quad \hat{L}_y = \begin{pmatrix} 0 & 0 & -i \\ 0 & 0 & 0 \\ i & 0 & 0 \end{pmatrix}, \quad \hat{L}_z = \begin{pmatrix} 0 & i & 0 \\ -i & 0 & 0 \\ 0 & 0 & 0 \end{pmatrix},$$

respectively. Here, we define the indices of \hat{L}_i and $\hat{\sigma}_j$ in Eq. (4) as $[i, j]$. $\Delta(T)$ is the pair potential at the temperature T and it has the Bardeen-Cooper-Schrieffer (BCS)-like temperature dependence,

$$\Delta(T) = \alpha_c \Delta_0 \tanh \left[1.74 \sqrt{\frac{T_c - T}{T}} \right], \quad (5)$$

$$\Delta_0 = \frac{3.53}{2} T_c, \quad (6)$$

with the critical temperature T_c . We choose α_c so that the maximal quasiparticle energy gap amplitude becomes Δ_0 , and its value is given in Appendix C (Table II). Likewise, for SSO pairings, we consider the spin-singlet pair potentials,

$$\hat{\Delta}(\mathbf{k}) = \Delta(T) [\hat{L}_i \otimes \hat{\sigma}_0 \sin k_{j=x,y,a}] i\hat{\sigma}_y, \quad (7)$$

$$\hat{\Delta}(\mathbf{k}) = \Delta(T) \left[\hat{L}_i \otimes \hat{\sigma}_0 \sin \frac{k_{j=zc}}{2} \right] i\hat{\sigma}_y, \quad (8)$$

with the lattice constants [a, a, c] and the definition of the indices \hat{L}_i and $k_{j=x,y,z}$ as $[i, j]$. Table I shows the classification of orbital-singlet pair potentials. We obtain 14 orbital-singlet pair potentials for both TSE and SSO states in the point group D_{4h} . Only interorbital E_g and E_u representations can break the TRS among the orbital-singlet pairings in Table I. The TRS broken pairings for TSE E_g $\{[z, x], [z, y]\}$ and $\{[x, z], [y, z]\}$ representations are written by the linear combination,

$$\hat{\Delta} = \Delta(T) [\hat{L}_z \otimes (\hat{\sigma}_x + i\hat{\sigma}_y)] i\hat{\sigma}_y, \quad (9)$$

$$\hat{\Delta} = \Delta(T) [(\hat{L}_x + i\hat{L}_y) \otimes \hat{\sigma}_z] i\hat{\sigma}_y, \quad (10)$$

respectively. Likewise, the time-reversal broken pairings for SSO E_u $\{[z, x], [z, y]\}$ and $\{[x, z], [y, z]\}$ representations are given by

$$\hat{\Delta}(\mathbf{k}) = \Delta(T) [\hat{L}_z \otimes \hat{\sigma}_0 (\sin k_x a + i \sin k_y a)] i\hat{\sigma}_y, \quad (11)$$

$$\hat{\Delta}(\mathbf{k}) = \Delta(T) \left[(\hat{L}_x + i\hat{L}_y) \otimes \hat{\sigma}_0 \sin \frac{k_z c}{2} \right] i\hat{\sigma}_y. \quad (12)$$

Spin susceptibility $\chi_i(T)$ along the $i = x, y, z$ axis at temperature T is given by the Kubo formula [64–66],

$$\begin{aligned} \chi_i(T) &= T \int_{\text{BZ}} d\mathbf{k} \sum_{i\varepsilon_n} \text{Tr}[\hat{s}_i \hat{g}(\mathbf{k}, i\varepsilon_n) \hat{s}_i \hat{g}(\mathbf{k}, i\varepsilon_n)] \quad (13) \\ &= \int_{\text{BZ}} d\mathbf{k} \sum_{\alpha, \beta} \langle \alpha | \hat{s}_i | \beta \rangle \langle \beta | \hat{s}_i | \alpha \rangle \\ &\quad \times T \sum_{i\varepsilon_n} G_\alpha(\mathbf{k}, i\varepsilon_n) G_\beta(\mathbf{k}, i\varepsilon_n) e^{+i\varepsilon_n 0}, \quad (14) \end{aligned}$$

TABLE I. Classification of the orbital-singlet pairings in the point group D_{4h} [45]. Spin-triplet/orbital-singlet/even-parity (TSE) pairing $\hat{\Delta} = \Delta(T)[\hat{L}_i \otimes \hat{\sigma}_j]i\hat{\sigma}_y$ is described by the \mathbf{d} -vector. Spin-singlet/orbital-singlet/odd-parity (SSO) pairing is expressed by the spin-singlet pair potential $\hat{\Delta}(\mathbf{k}) = \Delta(T)[\hat{L}_i \otimes \hat{\sigma}_0 \sin k_j]i\hat{\sigma}_y$ for $[i, j]$ ($i, j = x, y, z$). Here $[i, j]$ means the indices of \hat{L}_i and $\hat{\sigma}_j$ in TSE pairing, and \hat{L}_i and k_j in SSO, respectively. We focus on the even-frequency pair potential in this table.

Irreducible rep.	State	Pair potential $[i, j]$	Gap structure
A_{1g}	TSE	$[y, y] + [x, x]$	Fully gapped
A_{1g}	TSE	$[z, z]$	fully Gapped
A_{2g}	TSE	$[y, x] - [x, y]$	Gapless
B_{1g}	TSE	$[y, y] - [x, x]$	Line node in the diagonal directions
B_{2g}	TSE	$[y, x] + [x, y]$	Line node in the x and y directions
E_g	TSE	$\{[z, x], [z, y]\}$	Bogoliubov Fermi surface in $k_z = 0, 2\pi$ planes
E_g	TSE	$\{[x, z], [y, z]\}$	Bogoliubov Fermi surface in $k_z = 0, 2\pi$ planes [45]
A_{1u}	SSO	$[y, y] + [x, x]$	Fully gapped
A_{1u}	SSO	$[z, z]$	Line node in $k_z = 0, 2\pi$ planes
A_{2u}	SSO	$[y, x] - [x, y]$	Line node in the x and y directions
B_{1u}	SSO	$[y, y] - [x, x]$	Fully gapped
B_{2u}	SSO	$[y, x] + [x, y]$	Line node in the x and y directions
E_u	SSO	$\{[z, x], [z, y]\}$	Bogoliubov Fermi surface in zx and yz planes
E_u	SSO	$\{[x, z], [y, z]\}$	Bogoliubov Fermi surface in $k_z = 0, 2\pi$ planes

$$\hat{g}(\mathbf{k}, i\varepsilon_n) = \frac{1}{i\varepsilon_n - \hat{H}_{\text{BdG}}(\mathbf{k})}, \quad (15)$$

$$\hat{H}_{\text{BdG}}(\mathbf{k})|\alpha\rangle = E_\alpha(\mathbf{k})|\alpha\rangle, \quad (16)$$

where $\hat{s}_{i=x,y,z}$ are the spin angular momentum operators expanded in particle-hole space, $i\varepsilon_n = i(2n+1)\pi T$ is the fermionic Matsubara frequency, $E_{\alpha(\beta)}(\mathbf{k})$ is the Bogoliubov energy band, and $|\alpha(\beta)\rangle$ is the eigenstate corresponding to the Bogoliubov energy band $E_{\alpha(\beta)}(\mathbf{k})$ with the band indices α, β . Here, $\hat{g}(\mathbf{k}, i\varepsilon_n)$ stands for the matrix of the Green's function in the spin-orbital basis and $G_\alpha(\mathbf{k}, i\varepsilon_n)$ denotes the Green's function defined by

$$G_\alpha(\mathbf{k}, i\varepsilon_n) = \frac{1}{i\varepsilon_n - E_\alpha(\mathbf{k})}. \quad (17)$$

Here, we adopt the formulation,

$$T \sum_{i\varepsilon_n} G_\alpha(\mathbf{k}, i\varepsilon_n) G_\beta(\mathbf{k}, i\varepsilon_n) e^{+i\varepsilon_n 0} = \begin{cases} -\frac{1}{4T} \left[1 - \tanh^2 \frac{E_\alpha(\mathbf{k})}{2T} \right] & E_\alpha(\mathbf{k}) = E_\beta(\mathbf{k}) \\ -\frac{\tanh \frac{E_\alpha(\mathbf{k})}{2T} - \tanh \frac{E_\beta(\mathbf{k})}{2T}}{2[E_\alpha(\mathbf{k}) - E_\beta(\mathbf{k})]} & E_\alpha(\mathbf{k}) \neq E_\beta(\mathbf{k}) \end{cases}, \quad (18)$$

to sum up the Matsubara frequency from $-\infty$ to ∞ analytically. Although the Fermi surface along the z -axis is almost cylindrical [45] and the t_{2g} -orbital characters at the Fermi level are nearly independent of k_z [see also Appendix B (Fig. 3)], we need the integration of k_z for all representations in the actual calculation.

III. RESULTS AND DISCUSSION

We show the temperature dependence of the calculated spin susceptibility below the critical temperature T_c for the orbital-singlet pairings in the three-dimensional SRO model. Figure 1 shows the temperature dependence of the spin susceptibility $\chi_{i=x,z}(T)$ normalized by $\chi_i(T_c)$ where the direction of the applied field is along the x -axis for Figs. 1(a), 1(c), 1(e), 1(g), and 1(i), and the z -axis for Figs. 1(b), 1(d), 1(f), 1(h), and 1(j). The spin susceptibility along the y -direction is the same as that along the x -axis due to the fourfold rotational symmetry in the xy -plane. In Fig. 1, the pair potentials used in the calculation are interorbital TSE A_{1g} [Figs. 1(a) and 1(b)], A_{2g} [Figs. 1(c) and 1(d)], B_{1g} [Figs. 1(e) and 1(f)], B_{2g} [Figs. 1(g) and 1(h)], and E_g [Figs. 1(i) and 1(j)] representations. The calculation result for intra-orbital spin-singlet s -wave state (BCS state) is also shown for reference in Fig. 1 (black dotted line). Note that TSE $E_g \{[x, z], [y, z]\}$ representation with TRS breaking is one of the promising candidates of pairing symmetry in SRO and the resulting energy spectrum has the Bogoliubov Fermi surface in xy -plane [45]. It is also noted that nonzero atomic spin-orbit coupling needs to open the energy gap. For the TSE state in Fig. 1, spin susceptibility decreases as temperature decreases for any irreducible representation in Table. I for both the x - and z -directed applied magnetic fields. In addition, as the quasiparticle energy spectrum in interorbital pairings does not open the energy gap $\Delta(T)$ on the Fermi surface, even if $\Delta(T)$ is modified by α_c in the BdG Hamiltonian, the function of the spin susceptibility $\chi_i(T)$ for interorbital pairings is convex upwards, not downwards.

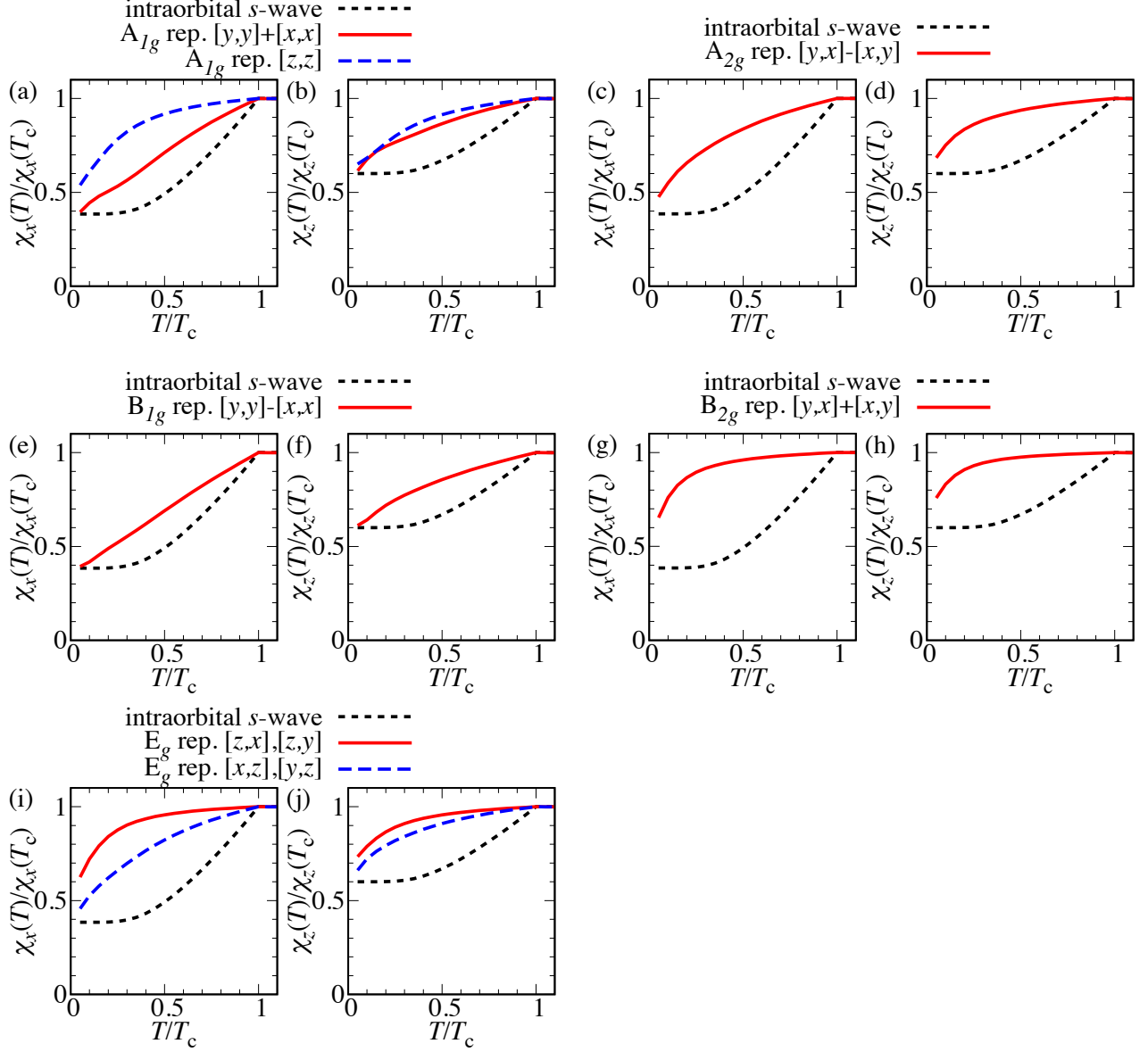


FIG. 1. Spin susceptibility $\chi_{i=x,z}(T)$ for intraorbital spin-singlet s -wave (black dotted line) and spin-triplet/orbital-singlet/ s -wave (TSE) pairings normalized by $\chi_i(T_c)$ along the (a), (c), (e), (g), and (i) x , and (b), (d), (f), (h), and (j) z -directions as a function of the temperature. As shown in Table I, we choose the pair potential as (a,b) TSE A_{1g} $[y, y] + [x, x]$ (red solid line) and $[z, z]$ (blue dotted line), (c,d) A_{2g} , (e,f) B_{1g} , (g,h) B_{2g} , and E_g $\{[z, x], [z, y]\}$ (red solid line) and $\{[x, z], [y, z]\}$ (blue dotted line) states, respectively. Here, we do not plot $\chi_y(T)/\chi_y(T_c)$ because spin susceptibility along the y direction $\chi_y(T)$ is the same as that along the x axis $\chi_x(T)$ in the presence of the fourfold rotational symmetry in the xy plane.

On the other hand, for the interorbital SSO pairings as shown in Fig. 2, the temperature dependence of the spin susceptibility is sensitive to the direction of the applied magnetic field. In the case of A_{1u} $[y, y] + [x, x]$ [red solid line in Figs. 2(a) and 2(b)], A_{2u} [Figs. 2(c) and 2(d)], B_{1u} [Figs. 2(e) and 2(f)], B_{2u} [Figs. 2(g) and 2(h)], and

E_u $\{[x, z], [y, z]\}$ [red solid line in Figs. 2(i) and 2(j)], the spin susceptibility decreases $\sim 50\%$ when the direction of the field is in the in-plane, and $\sim 5\%$ along z -axis, as shown in Fig. 2. In contrast, spin susceptibility for SSO A_{1u} $[z, z]$ [blue dotted line in Figs. 2(a) and 2(b)] and E_u $\{[z, x], [z, y]\}$ [blue dotted line in Figs. 2(i) and

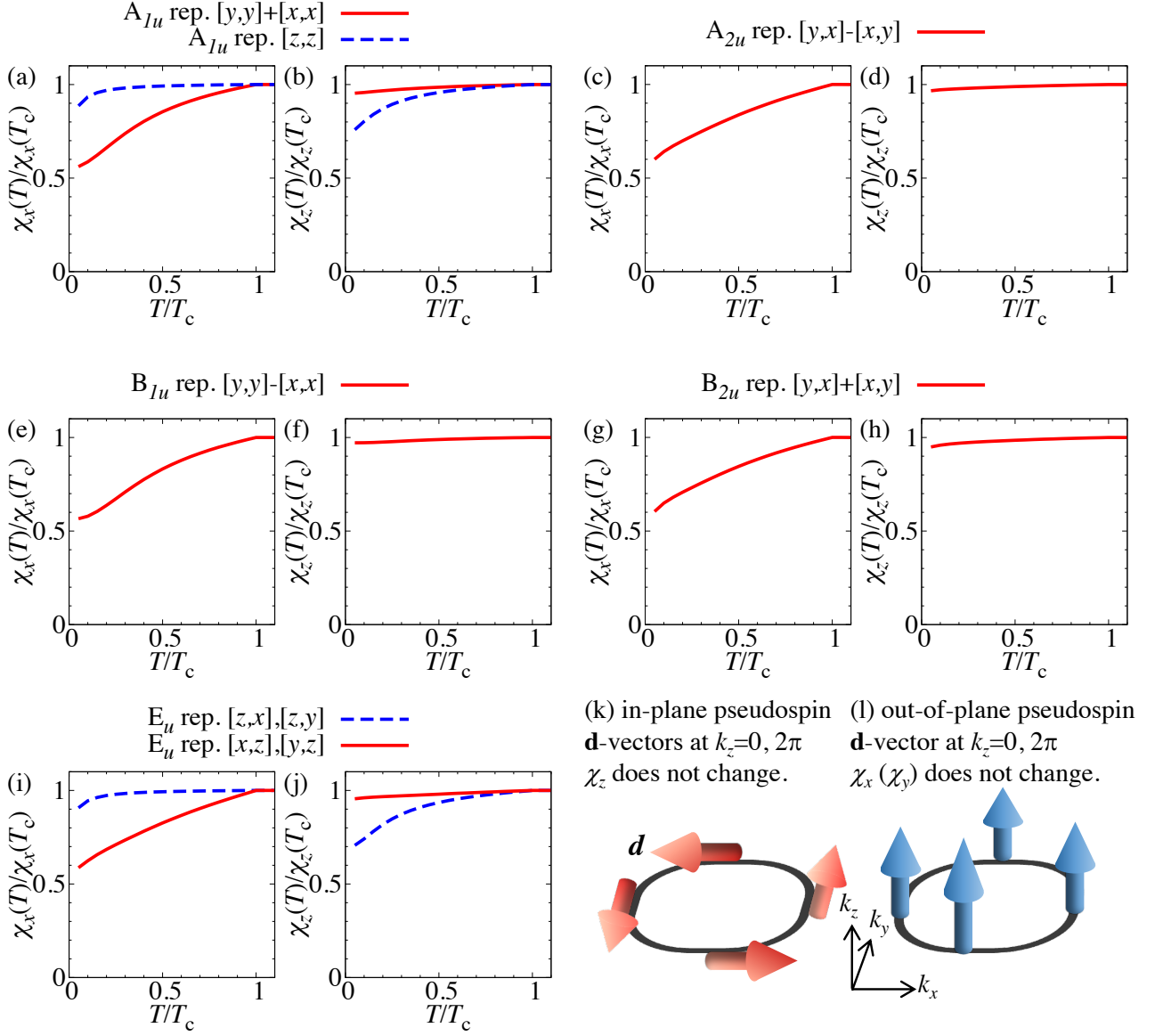


FIG. 2. Spin susceptibility $\chi_{i=x,z}(T)$ for spin-singlet/orbital-singlet/odd-parity (SSO) pairings normalized by $\chi_i(T_c)$ along the (a), (c), (e), (g), and (i) x , and (b), (d), (f), (h), and (j) z axes as a function of the temperature. As shown in Table. I, we select the pair potential as (a,b) SSO A_{1u} $[y, y] + [x, x]$ (red solid line) and $[z, z]$ (blue dotted line), (c,d) A_{2u} , (e,f) B_{1g} , (g,h) B_{2u} , and (i,j) E_u $\{[z, x], [z, y]\}$ (blue dotted line) and $\{[x, z], [y, z]\}$ (red solid) states, respectively. Schematic illustration of (k) in-plane and (l) out-of-plane pseudospin \mathbf{d} -vectors in the band basis at $k_z = 0, 2\pi$. Black line means the Fermi line. Away from the xy -symmetric plane, pseudospin \mathbf{d} -vector is not aligned in the xy plane and along the z axis, respectively.

2(j)] representations decreases for the magnetic field in the z -direction, as well as $\sim 10\%$ along the x -axis at low temperature. These results contradict naive understanding for the single-band results where spin susceptibility decreases for any direction of the field in a spin-singlet pairing or along the direction parallel to the \mathbf{d} -vector of the pair potential.

To resolve this, we focus on the pseudospin state in the band basis and parity dependence for each orbital-singlet pair potential. In principle, when the spin-singlet/even-parity pairing is realized in the single orbital model, spin

susceptibility goes to zero at $T = 0$ irrespective of the direction of the magnetic field. In the spin-triplet/odd-parity pairing, the spin susceptibility is reduced below T_c if the \mathbf{d} -vector is parallel to the magnetic field. However, when the \mathbf{d} -vector is perpendicular to the magnetic field, spin susceptibility does not change with the temperature. It implies that we can determine the spin structure by the temperature dependence of the spin susceptibility in the single-orbital model. In the present study, spin susceptibility for TSE (SSO) pairings is reduced independently of the direction of the applied mag-

netic fields (has the anisotropic behavior for the directions). For TSE pairings, the temperature dependence shown in Fig. 1 is caused by the pseudospin-singlet state in the band basis, despite the spin-triplet pairing in the spin-orbital space. We note that spin susceptibility does not go to zero at $T = 0$ due to the Van-Vleck paramagnetism in the presence of the atomic spin-orbit coupling. In SSO pairings as shown in Fig. 2, we can adopt the \mathbf{d} -vector that describes the pseudospin-triplet state. As shown in Fig. 2, the spin susceptibility decreases 5-10% along the direction where there is no reduction in the single-orbital model. In the present study, this pseudospin \mathbf{d} -vector is not perfectly aligned in the xy -plane or along the z -axis away from the xy -symmetric plane owing to the strong atomic spin-orbit coupling. Since the pseudospin \mathbf{d} -vector is almost in-plane in the SSO $A_{1u} [y, y] + [x, x]$, A_{2u} , B_{1u} , B_{2u} , and $E_u \{[x, z], [y, z]\}$ representations, the spin susceptibility changes around 5% along the z -axis. For the $A_{1u} [z, z]$ and $E_u \{[z, x], [z, y]\}$ representations, the pseudospin \mathbf{d} -vector is out-of-plane and it is not parallel to the z -axis. Thus, spin susceptibility in the $A_{1u} [z, z]$ and $E_u \{[z, x], [z, y]\}$ pairings is reduced $\sim 10\%$ by in-plane applied magnetic field at low temperature. These behaviors also occur even in the intraorbital spin-triplet/odd-parity and the interorbital TTO pairings. We show the spin susceptibility for the intraorbital chiral p -wave pairing in Appendix F, on behalf of all spin-triplet/odd-parity states. The spin susceptibility along the z -direction does not become zero owing to the strong atomic spin-orbit coupling in the interorbital $A_{1u} [z, z]$ and $E_u \{[z, x], [z, y]\}$ states.

Here, we point out the relation between spin susceptibility and pseudospin/parity state. The behavior with the temperature in TSE (SSO) pairings is similar to that in spin-singlet/even-parity (spin-triplet/odd-parity). We can mention that the symmetry of the parity coincides with the temperature dependence of the spin susceptibility for the orbital-singlet pair potential. Therefore, in multiorbital SCs with strong atomic spin-orbit coupling, the temperature dependence of the spin susceptibility for the orbital-singlet Cooper pair is determined by the pseudospin/parity state in the band basis. For this perspective, we can mention that spin susceptibility for orbital-singlet pairings with different momentum dependence, e.g., TSE d and SSO f -wave, behaves qualitatively the same as that for s and p -wave cases in the present study, respectively. We note that these kinds of temperature dependence for orbital-singlet pairings in the present study are the same as a theoretical research of the spin susceptibility in the superconducting topological insulator $\text{Cu}_x\text{Bi}_2\text{Se}_3$ [66].

IV. SUMMARY AND CONCLUSION

We studied the temperature dependence of the spin susceptibility below T_c for the orbital-singlet Cooper pair in SRO. The pseudospin state in the band basis is de-

termined by the parity of the pair potential. In other words, the pseudospin-singlet (triplet) state is realized in the case of even (odd) parity pairing. If we consider orbital-singlet pairing, pseudospin-singlet (triplet) state means spin-triplet (singlet) pairing. Thus, the spin susceptibility for the spin-triplet/orbital-singlet/ s -wave pairings decreases with the temperature, independently of the direction of the applied magnetic fields. In the spin-singlet/orbital-singlet/odd-parity pairings, the spin susceptibility decreases around 5% (10%) along the z (x) axis for $A_{1u} [y, y] + [x, x]$, A_{2u} , B_{1u} , B_{2u} , and $E_u \{[x, z], [y, z]\}$ ($A_{1u} [z, z]$, and $E_u \{[z, x], [z, y]\}$) representations at low temperature. It is caused by the pseudospin \mathbf{d} -vector that is not completely aligned in the xy -plane (along the z -direction) away from the xy -symmetric plane due to the strong atomic spin-orbit coupling. This behavior is relevant to the effect of the atomic spin-orbit coupling, not the orbital nature in the superconducting state. Here, the quantitative of the spin susceptibility strongly depends on the length of the atomic spin-orbit coupling, as the importance of the strong spin-orbit coupling in SRO was pointed out [56, 57]. Based on the present study, the recent NMR experiments [31–33] indicate not the spin-singlet pairing, but the pseudospin-singlet/even-parity one in SRO. At least, since the spin-triplet/orbital-singlet/ s -wave pairings are pseudospin-singlet states, they do not contradict the recent NMR experiments [31–33]. Likewise, the spin susceptibility for accidentally degenerate intraorbital spin-singlet pairings [38–44], that behaves the same as that for the intraorbital spin-singlet cases, is also consistent with these NMR experiments. To elucidate the pairing symmetry of the spin-degree of freedom of the present spin-triplet/orbital-singlet/even-parity and spin-singlet/orbital-singlet/odd-parity pairings, charge transport in SC/ferromagnet junctions with a well-oriented interface is highly desired [67, 68] because tunneling spectroscopy via Andreev bound states plays an important role in the determination of the unconventional superconductors [69, 70].

V. ACKNOWLEDGEMENTS

This work is supported by the JSPS KAKENHI (Grants No. JP15H05851, No. JP15H05853, No. JP15K21717, No. JP18H01176, No. JP18K03538, No. JP20H00131, and No. JP20H01857) from MEXT of Japan, Researcher Exchange Program between JSPS and RFBR (Grants No. JPJSBP120194816), and the JSPS Core-to-Core program Oxide Superspin international network (Grants No. JPJSCCA20170002). We thank Y. Maeno, P. Gentile, and H. Kaneyasu for the helpful comments. We also appreciate the valuable comments and discussions by H. G. Suh and D. F. Agterberg.

Appendix A: Model Hamiltonian of three-dimensional Sr₂RuO₄ in the normal state

In Appendix A, we describe the three-dimensional Hamiltonian of Sr₂RuO₄ (SRO) in the normal state in Refs. [43, 45, 49, 56–58]. Gell-Mann matrices $\hat{\Lambda}_{l=0\sim 8}$ are defined by

$$\begin{aligned}\hat{\Lambda}_0 &= \begin{pmatrix} 1 & 0 & 0 \\ 0 & 1 & 0 \\ 0 & 0 & 1 \end{pmatrix}, \quad \hat{\Lambda}_1 = \begin{pmatrix} 0 & 1 & 0 \\ 1 & 0 & 0 \\ 0 & 0 & 0 \end{pmatrix}, \\ \hat{\Lambda}_2 &= \begin{pmatrix} 0 & 0 & 1 \\ 0 & 0 & 0 \\ 1 & 0 & 0 \end{pmatrix}, \quad \hat{\Lambda}_3 = \begin{pmatrix} 0 & 0 & 0 \\ 0 & 0 & 1 \\ 0 & 1 & 0 \end{pmatrix}, \\ \hat{\Lambda}_4 &= \begin{pmatrix} 0 & -i & 0 \\ i & 0 & 0 \\ 0 & 0 & 0 \end{pmatrix}, \quad \hat{\Lambda}_5 = \begin{pmatrix} 0 & 0 & -i \\ 0 & 0 & 0 \\ i & 0 & 0 \end{pmatrix}, \\ \hat{\Lambda}_6 &= \begin{pmatrix} 0 & 0 & 0 \\ 0 & 0 & -i \\ 0 & i & 0 \end{pmatrix}, \quad \hat{\Lambda}_7 = \begin{pmatrix} 1 & 0 & 0 \\ 0 & -1 & 0 \\ 0 & 0 & 0 \end{pmatrix}, \\ \hat{\Lambda}_8 &= \frac{1}{\sqrt{3}} \begin{pmatrix} 1 & 0 & 0 \\ 0 & 1 & 0 \\ 0 & 0 & -2 \end{pmatrix},\end{aligned}$$

in the $[d_{yz}, d_{zx}, d_{xy}]$ basis. We note that the Gell-Mann matrices $\hat{\Lambda}_{l=4,5,6}$ correspond to the t_{2g} -orbital angular momentum operators,

$$\hat{L}_x = -\hat{\Lambda}_6, \quad \hat{L}_y = \hat{\Lambda}_5, \quad \hat{L}_z = -\hat{\Lambda}_4,$$

respectively. The matrix elements $h_{lj}(\mathbf{k})$ are given by

$$h_{00}(\mathbf{k}) = \frac{1}{3}[\xi_{yz}(\mathbf{k}) + \xi_{zx}(\mathbf{k}) + \xi_{xy}(\mathbf{k})], \quad (\text{A1})$$

$$h_{70}(\mathbf{k}) = \frac{1}{2}[\xi_{yz}(\mathbf{k}) - \xi_{zx}(\mathbf{k})], \quad (\text{A2})$$

$$h_{80}(\mathbf{k}) = \frac{1}{2\sqrt{3}}[\xi_{yz}(\mathbf{k}) + \xi_{zx}(\mathbf{k}) - 2\xi_{xy}(\mathbf{k})], \quad (\text{A3})$$

with intraorbital hopping terms,

$$h_{10}(\mathbf{k}) = g(\mathbf{k}), \quad (\text{A4})$$

$$h_{20}(\mathbf{k}) = 8t_z^{(zx,xy)} \sin \frac{k_z c}{2} \sin \frac{k_x a}{2} \cos \frac{k_y a}{2}, \quad (\text{A5})$$

$$h_{30}(\mathbf{k}) = 8t_z^{(zx,xy)} \sin \frac{k_z c}{2} \cos \frac{k_x a}{2} \sin \frac{k_y a}{2}, \quad (\text{A6})$$

with interorbital hopping,

$$h_{43}(\mathbf{k}) = -\lambda_z, \quad (\text{A7})$$

$$h_{52}(\mathbf{k}) = -h_{61}(\mathbf{k}) = \lambda_{xy}, \quad (\text{A8})$$

with isotropic atomic spin-orbit coupling $\lambda_z = \lambda_{xy} = \lambda_{\text{SO}}$, and

$$h_{52}(\mathbf{k}) = h_{61}(\mathbf{k}) = 2\lambda_{5261}^{\text{SOC}} [\cos k_x a - \cos k_y a], \quad (\text{A9})$$

$$h_{51}(\mathbf{k}) = -h_{62}(\mathbf{k}) = 4\lambda_{5162}^{\text{SOC}} \sin k_x a \sin k_y a, \quad (\text{A10})$$

$$h_{41}(\mathbf{k}) = 8\lambda_{12z}^{\text{SOC}} \sin \frac{k_z c}{2} \sin \frac{k_x a}{2} \cos \frac{k_y a}{2}, \quad (\text{A11})$$

$$h_{42}(\mathbf{k}) = 8\lambda_{12z}^{\text{SOC}} \sin \frac{k_z c}{2} \cos \frac{k_x a}{2} \sin \frac{k_y a}{2}, \quad (\text{A12})$$

$$h_{63}(\mathbf{k}) = -8\lambda_{56z}^{\text{SOC}} \sin \frac{k_z c}{2} \sin \frac{k_x a}{2} \cos \frac{k_y a}{2}, \quad (\text{A13})$$

$$h_{53}(\mathbf{k}) = 8\lambda_{56z}^{\text{SOC}} \sin \frac{k_z c}{2} \cos \frac{k_x a}{2} \sin \frac{k_y a}{2}, \quad (\text{A14})$$

with \mathbf{k} -dependent spin-orbit coupling, respectively. Here, $\xi_{yz,zx,xy}(\mathbf{k})$ and $g(\mathbf{k})$ are described by

$$\begin{aligned}\xi_{yz}(\mathbf{k}) &= -\mu_z + 2t_y^{(z,z)} \cos k_x a + 2t_x^{(z,z)} \cos k_y a \\ &\quad + 8t_z^{(z,z)} \cos \frac{k_x a}{2} \cos \frac{k_y a}{2} \cos \frac{k_z c}{2} \\ &\quad + 4t_{xy}^{(z,z)} \cos k_x a \cos k_y a\end{aligned} \quad (\text{A15})$$

$$\begin{aligned}&\quad + 2t_{yy}^{(z,z)} \cos 2k_x a + 2t_{xx}^{(z,z)} \cos 2k_y a \\ &\quad + 4t_{xy}^{(z,z)} \cos 2k_x a \cos k_y a + 4t_{xy}^{(z,z)} \cos 2k_y a \cos k_x a \\ &\quad + 2t_{zz}^{(z,z)} (\cos k_z a - 1),\end{aligned} \quad (\text{A16})$$

$$\begin{aligned}\xi_{zx}(\mathbf{k}) &= -\mu_z + 2t_x^{(z,z)} \cos k_x a + 2t_y^{(z,z)} \cos k_y a \\ &\quad + 8t_z^{(z,z)} \cos \frac{k_x a}{2} \cos \frac{k_y a}{2} \cos \frac{k_z c}{2} \\ &\quad + 4t_{xy}^{(z,z)} \cos k_x a \cos k_y a \\ &\quad + 2t_{xx}^{(z,z)} \cos 2k_x a + 2t_{yy}^{(z,z)} \cos 2k_y a \\ &\quad + 4t_{xy}^{(z,z)} \cos 2k_x a \cos k_y a + 4t_{xy}^{(z,z)} \cos 2k_y a \cos k_x a \\ &\quad + 2t_{zz}^{(z,z)} (\cos k_z c - 1),\end{aligned} \quad (\text{A17})$$

$$\begin{aligned}\xi_{xy}(\mathbf{k}) &= -\mu_{xy} + 2t_x^{(xy,xy)} (\cos k_x a + \cos k_y a) \\ &\quad + 8t_z^{(xy,xy)} \cos \frac{k_x a}{2} \cos \frac{k_y a}{2} \cos \frac{k_z c}{2} \\ &\quad + 4t_{xy}^{(xy,xy)} \cos k_x a \cos k_y a \\ &\quad + 2t_{xx}^{(xy,xy)} (\cos 2k_x a + \cos 2k_y a) \\ &\quad + 4t_{xy}^{(xy,xy)} (\cos 2k_x a \cos k_y a + \cos 2k_y a \cos k_x a) \\ &\quad + 2t_{zz}^{(xy,xy)} (\cos k_z c - 1),\end{aligned} \quad (\text{A18})$$

$$\begin{aligned}g(\mathbf{k}) &= 8t_z^z \sin \frac{k_x a}{2} \sin \frac{k_y a}{2} \cos \frac{k_z c}{2} \\ &\quad - 4t_{xy}^z \sin k_x a \sin k_y a \\ &\quad - 4t_{xy}^z (\sin 2k_x a \sin k_y a + \sin 2k_y a \sin k_x a).\end{aligned} \quad (\text{A19})$$

We set the parameters as shown in Table II [45] and fix $T_c = 1.0 \times 10^{-4}t$ with $|t_x^{(xy,xy)}| = t$.

TABLE II. Parameters in three-dimensional Sr_2RuO_4 model in Ref. [45]. We set all values in meV.

$t_x^{(z,z)} = -362.4$	$t_y^{(z,z)} = -134$	$t_x^{(xy,xy)} = -262.4$	$t_{xy}^{(z,z)} = -44.01$	$t_{xx}^{(z,z)} = -1.021$	$t_{yy}^{(z,z)} = -5.727$	$t_{xy}^{(xy,xy)} = -43.73$
$t_{xx}^{(xy,xy)} = 34.23$	$t_{xy}^z = 16.25$	$t_{xx}^{(z,z)} = -13.93$	$t_{xy}^{(z,z)} = -7.52$	$t_{xx}^{(xy,xy)} = 8.069$	$t_{xx}^z = 3.94$	$\lambda_{\text{SO}} = 57.39$
$\mu_z = 438.5$	$\mu_{xy} = 218.6$	$t_z^{(z,z)} = -0.0228$	$t_z^{(xy,xy)} = 1.811$	$t_z^z = 9.975$	$t_z^{(z,xy)} = 8.304$	$t_{zz}^{(z,z)} = 2.522$
$t_{zz}^{(xy,xy)} = -3.159$	$\lambda_{56z}^{\text{SOC}} = -1.247$	$\lambda_{12z}^{\text{SOC}} = -3.576$	$\lambda_{516z}^{\text{SOC}} = -1.008$	$\lambda_{5261}^{\text{SOC}} = 0.3779$		

TABLE III. $\Delta_{\text{eff}}/\Delta_0$ for each energy band. We choose the maximum value of $\Delta_{\text{eff}}/\Delta_0$ as $\alpha_c = \Delta_0/\Delta_{\text{eff}}$. For the interorbital A_{2g} representation, the gapless state appears.

Irreducible rep.	State	Gap function	α -band	γ -band	β -band
A_{1g}	TSE	$[y, y] + [x, x]$	0.167	1.01	1.27
A_{1g}	TSE	$[z, z]$	0.904	0.751	0.314
A_{2g}	TSE	$[y, x] - [x, y]$	8.65×10^{-3}	4.69×10^{-2}	4.11×10^{-2}
B_{1g}	TSE	$[y, y] - [x, x]$	0.227	1.00	0.745
B_{2g}	TSE	$[y, x] + [x, y]$	0.221	0.329	7.28×10^{-2}
E_g	TSE	$\{[z, x], [z, y]\}$	0.404	0.457	4.00×10^{-2}
E_g	TSE	$\{[x, z], [y, z]\}$	0.163	0.314	0.235
A_{1u}	SSO	$[y, y] + [x, x]$	0.213	0.672	0.850
A_{1u}	SSO	$[z, z]$	0.949	0.795	0.265
A_{2u}	SSO	$[y, x] - [x, y]$	9.36×10^{-2}	1.00	1.00
B_{1u}	SSO	$[y, y] - [x, x]$	0.172	0.832	0.912
B_{2u}	SSO	$[y, x] + [x, y]$	0.194	0.967	0.964
E_u	SSO	$\{[z, x], [z, y]\}$	1.13	1.07	0.428
E_u	SSO	$\{[x, z], [y, z]\}$	0.144	0.960	0.748

Appendix B: Orbital characters at the Fermi level in three-dimensional Sr_2RuO_4 model

Next, we confirm the orbital characters in the normal state at the Fermi level in the three-orbital SRO model in Refs. [45, 57]. Here, we consider the density of states for each t_{2g} -orbital on the Fermi surface,

$$N_\alpha(\mathbf{k}, E_F) = -\frac{1}{\pi} \text{Im} [G_{\alpha\uparrow, \alpha\uparrow}(\mathbf{k}, E_F + i\delta) + G_{\alpha\downarrow, \alpha\downarrow}(\mathbf{k}, E_F + i\delta)], \quad (\text{B1})$$

$$\hat{G}(\mathbf{k}, E_F) = \frac{1}{E_F + i\delta - \hat{H}(\mathbf{k})}, \quad (\text{B2})$$

with the diagonal elements of the retarded Green's function in the normal state $G_{\alpha\uparrow, \alpha\uparrow}(\mathbf{k}, E_F + i\delta)$ and $G_{\alpha\downarrow, \alpha\downarrow}(\mathbf{k}, E_F + i\delta)$, t_{2g} -orbital indices $\alpha = yz, zx, xy$, the Fermi energy E_F , and the infinitesimal value δ . In Figs. 3(a), 3(b), and 3(c), we plot the orbital characters at the Fermi level in Fig. 3(a) $k_z = 0$, Fig. 3(b) $k_z = \pi/2$, Fig. 3(c) $k_z = \pi$, and Fig. 3(d) $k_z = 2\pi$ planes by calculating the density of states for each t_{2g} -orbital in the normal state. Since the Fermi surface is cylindrical along

the k_z -direction, t_{2g} -orbital characters are almost independent of k_z .

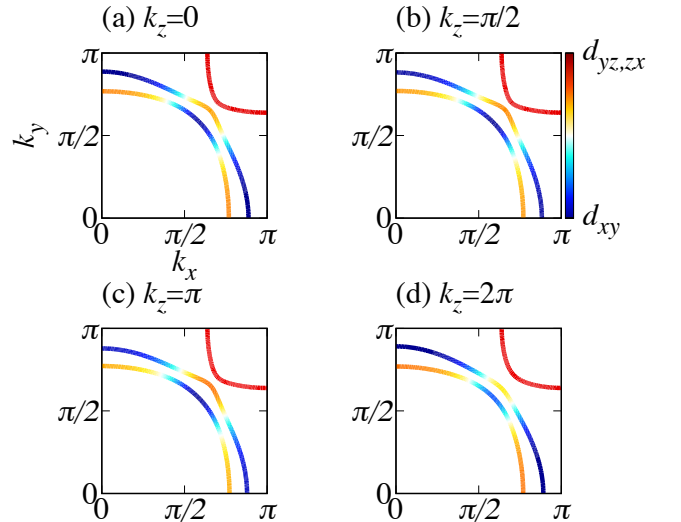


FIG. 3. t_{2g} -orbital characters in the normal state at the Fermi level in (a) $k_z = 0$, (b) $k_z = \pi/2$, (c) $k_z = \pi$, and (d) $k_z = 2\pi$ planes.

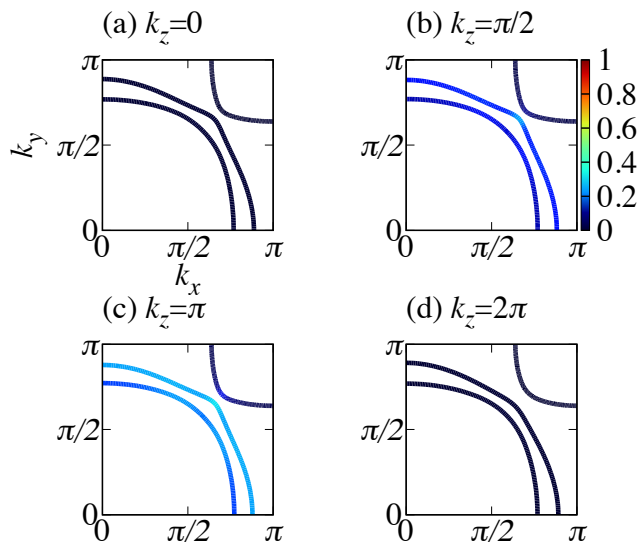


FIG. 4. Gap structure of the orbital-singlet E_g $\{[x, z], [y, z]\}$ pairing in Eq. (10) at the Fermi level at (a) $k_z = 0$, (b) $k_z = \pi/2$, (c) $k_z = \pi$, and (d) $k_z = 2\pi$. We set the temperature at $T = 0$. Color bar indicates the gap amplitude normalized by Δ_0 .

Appendix C: Setting of value α_c

Third, we summarize the constant value α_c for each energy band. In SRO, the energy dispersion is described by the lowest energy band α , γ , and the highest one β . We set the constant value α_c as

$$\alpha_c = \frac{\Delta_0}{\Delta_{\text{eff}}}, \quad (\text{C1})$$

where Δ_{eff} is the magnitude of the actual maximum gap amplitude when we set Δ_0 in the gap function. Table III shows the value of $\Delta_{\text{eff}}/\Delta_0$ for each energy band, α , γ , and β . Since we obtain the maximum gap amplitude by the magnitude of the actual opening energy gap in experiments, we modify the gap amplitude $\Delta(T)$ by using α_c . We choose the maximum value of $\Delta_{\text{eff}}/\Delta_0$ as $\alpha_c = \Delta_0/\Delta_{\text{eff}}$ for each irreducible representation.

Appendix D: Gap structure of orbital-singlet E_g pairing $\{[x, z], [y, z]\}$ on the Fermi surface

In Appendix D, we confirm the gap structure in interorbital E_g $\{[x, z], [y, z]\}$ pairing on the Fermi surface. Here, we choose the pair potential as Eq. (10). Fig. 4 shows the eigenvalues of the BdG Hamiltonian at the Fermi level at $k_z = 0$ [Fig. 4(a)], $k_z = \pi/2$ [Fig. 4(b)], $k_z = \pi$ [Fig. 4(c)], and $k_z = 2\pi$ [Fig. 4(d)]. In our calculation, since we select the lower critical temperature $T_c/t = 1.0 \times 10^{-4}$, we do not obtain the same gap structure in Ref. [45].

Appendix E: Spin susceptibility for interorbital spin-singlet/orbital-triplet pairings

In Appendix E, we investigate the spin susceptibility for interorbital spin-singlet/orbital-triplet/ s -wave (STE) pairings. The interorbital STE state appears for B_{2g} and E_g representations in Ref. [45]. Figure 5 plots the spin susceptibility $\chi_{i=x,z}(T)$ as a function of the temperature along the x [Figs. 5(a) and 5(c)] and z -directions [Figs. 5(b) and 5(d)] for STE B_{2g} [Figs. 5(a) and 5(c)] and E_g representations [Figs. 5(b) and 5(d)]. As well as spin-triplet/orbital-singlet/ s -wave pairings, the spin susceptibility for interorbital spin-singlet/orbital-triplet/ s -wave pairings decreases with the temperature, independently of the axis of the applied magnetic field, owing to the pseudospin-singlet state in the band basis.

Appendix F: Spin susceptibility for intraorbital chiral p -wave pairing

Finally, we calculate the spin susceptibility for the intrarorbital chiral p -wave pairing, on behalf of all spin-triplet/odd-parity states. The chiral p -wave state in the present study is given by

$$\hat{\Delta}(\mathbf{k}) = \Delta(T) \hat{L}_0 \otimes \hat{\sigma}_z [\sin k_x + i \sin k_y] i \hat{\sigma}_y, \quad (\text{F1})$$

with the unit matrix in t_{2g} -orbital space \hat{L}_0 .

Figure 6 plots the spin susceptibility $\chi_{i=x,z}(T)$ for the intraorbital chiral p -wave state as a function of the temperature at nonzero λ_{SO} in Table II [Figs. 6(a) to 6(c)] and $\lambda_{\text{SO}}/t = 0$ [Figs. 6(d) to 6(f)]. It includes the k_z -resolved spin susceptibility $\chi'_{i=x,z}(T, k_z)$ at (b)(e) $k_z = 0$ [Figs. 6(b) and 6(e)] and $k_z = 1.2\pi$ [Figs. 6(c) and 6(f)]. Here, the spin susceptibility $\chi_{i=x,z}(T)$ is described by

$$\chi_i(T) \sim \int_{-2\pi}^{2\pi} \chi'_{i=x,z}(T, k_z) dk_z. \quad (\text{F2})$$

The spin susceptibility at nonzero atomic spin-orbit coupling λ_{SO} decreases around 5% along the x -direction at low temperature as shown in Fig. 6(a). To analyze this behavior, we resolve the spin susceptibility for k_z . Then we select $k_z = 0$ and $k_z = 1.2\pi$. Because the k_z -resolved spin susceptibility along the x -axis changes remarkably when k_z is larger than π , we choose $k_z = 1.2\pi$ in Fig. 6. At $k_z = 0$, the k_z -resolved spin susceptibility does not change along the x -direction as shown in Fig. 6(b). As $k_z = 0$ ($k_z = 2\pi$) is on the symmetric line (the edge of the Brillouin zone), the pseudospin \mathbf{d} -vector should be aligned along the x -axis in the intraorbital chiral p -wave pairing. However, the k_z -resolved spin susceptibility at $k_z = 1.2\pi$ decreases around 10% along the x -axis as shown in Fig. 6(c). Thus, the spin susceptibility is reduced along the x -direction by the components away from the xy -symmetric plane.

To unveil the role of the atomic spin-orbit coupling λ_{SO} , we also study the spin susceptibility at $\lambda_{\text{SO}}/t = 0$.

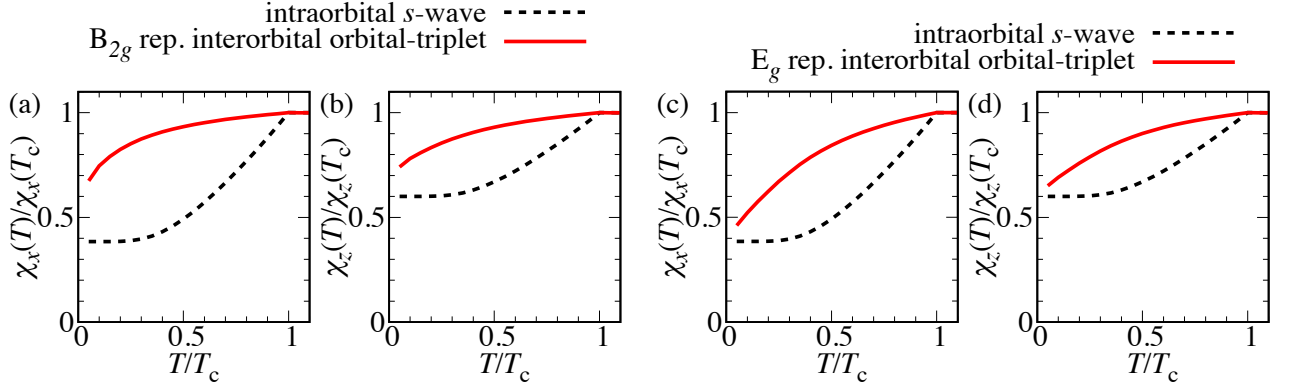


FIG. 5. Spin susceptibility $\chi_{i=x,z}(T)$ for interorbital STE (a)(b) B_{2g} and (c)(d) E_g pairings normalized by $\chi_i(T_c)$ along the (a)(c) x and (b)(d) z -directions as a function of the temperature.

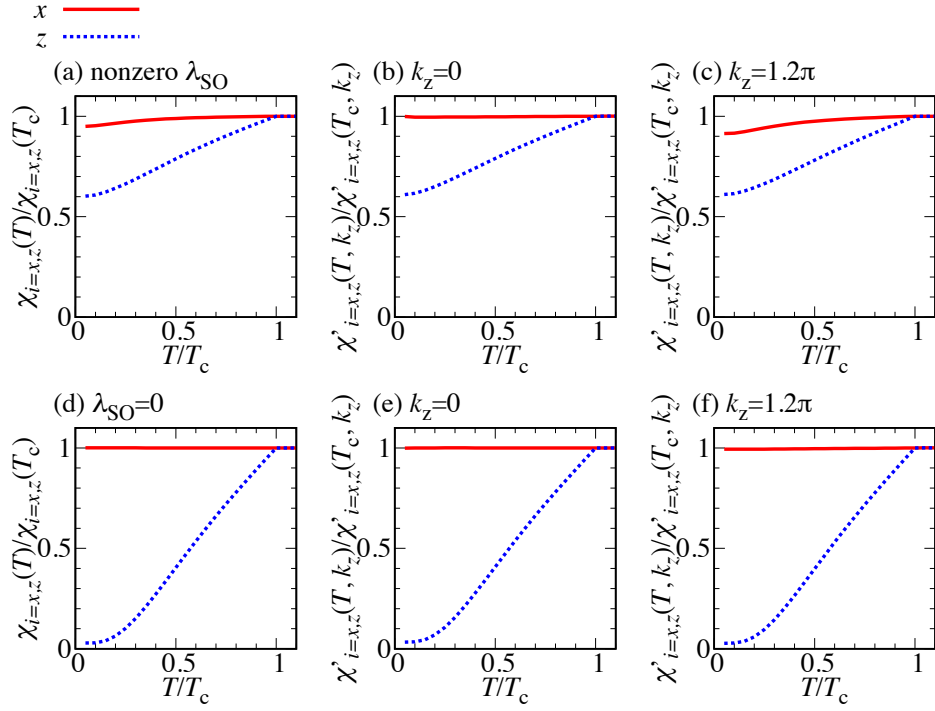


FIG. 6. Spin susceptibility for the intraorbital chiral p -wave pairing at (a) nonzero λ_{SO} and (d) $\lambda_{SO}/t = 0$, normalized by $\chi_i(T_c)$ along the x (red solid line) and z -directions (blue dotted line) as a function of the temperature. k_z -resolved spin susceptibility $\chi_{i=x,z}(T)$ for the intraorbital chiral p -wave pairing at (b)(c) nonzero λ_{SO} and (e)(f) $\lambda_{SO}/t = 0$. We fix k_z as (b)(e) $k_z = 0$ and (c)(f) $k_z = 1.2\pi$. We set the value of nonzero λ_{SO} as shown in Table II.

At $\lambda_{SO}/t = 0$, the spin susceptibility does not decrease along the x -direction in Fig. 6(d). Since the pseudospin \mathbf{d} -vector for the chiral p -wave pairing is completely aligned along the z -axis for all k_z , the k_z -resolved spin susceptibility at both $k_z = 0$ and 1.2π does not change along the x -axis as shown in Figs. 6(e) and 6(f).

In conclusion, at the nonzero atomic spin-orbit cou-

pling λ_{SO} , when we can define the pseudospin \mathbf{d} -vector, the spin susceptibility is reduced around 5-10% along the axis where there is no reduction in the single-orbital model. It occurs by the pseudospin \mathbf{d} -vector that is not completely aligned in the xy -plane or z -direction away from the xy -symmetric plane in the presence of the strong atomic spin-orbit coupling λ_{SO} .

- [1] Y. Maeno, H. Hashimoto, K. Yoshida, S. Nishizaki, T. Fujita, J. G. Bednorz, and F. Lichtenberg, Superconductivity in a layered perovskite without copper, *Nature* **372**, 532 (1994).
- [2] A. P. Mackenzie and Y. Maeno, The superconductivity of Sr_2RuO_4 and the physics of spin-triplet pairing, *Rev. Mod. Phys.* **75**, 657 (2003).
- [3] Y. Maeno, S. Kittaka, T. Nomura, S. Yonezawa, and K. Ishida, Evaluation of spin-triplet superconductivity in Sr_2RuO_4 , *J. Phys. Soc. Jpn.* **81**, 011009 (2012).
- [4] J. A. Duffy, S. M. Hayden, Y. Maeno, Z. Mao, J. Kulda, and G. J. McIntyre, Polarized-neutron scattering study of the cooper-pair moment in Sr_2RuO_4 , *Phys. Rev. Lett.* **85**, 5412 (2000).
- [5] J. Jang, D. Ferguson, V. Vakaryuk, R. Budakian, S. Chung, P. Goldbart, and Y. Maeno, Observation of half-height magnetization steps in Sr_2RuO_4 , *Science* **331**, 186 (2011).
- [6] Y. Yasui, K. Lahabi, M. S. Anwar, Y. Nakamura, S. Yonezawa, T. Terashima, J. Aarts, and Y. Maeno, Little-parks oscillations with half-quantum fluxoid features in Sr_2RuO_4 microrings, *Phys. Rev. B* **96**, 180507(R) (2017).
- [7] M. Yamashiro, Y. Tanaka, and S. Kashiwaya, Theory of the d.c. josephson effect in s -wave/ p -wave/ s -wave superconductor junction, *J. Phys. Soc. Jpn.* **67**, 3364 (1998).
- [8] R. Jin, Y. Zadorozhny, Y. Liu, D. G. Schlom, Y. Mori, and Y. Maeno, Observation of anomalous temperature dependence of the critical current in $\text{Pb}/\text{Sr}_2\text{RuO}_4/\text{Pb}$ junctions, *Phys. Rev. B* **59**, 4433 (1999).
- [9] F. Laube, G. Goll, H. v. Löhneysen, M. Fogelström, and F. Lichtenberg, Spin-triplet superconductivity in Sr_2RuO_4 probed by andreev reflection, *Phys. Rev. Lett.* **84**, 1595 (2000).
- [10] Y. Tanaka, T. Yokoyama, A. V. Balatsky, and N. Nagaosa, Theory of topological spin current in non-centrosymmetric superconductors, *Phys. Rev. B* **79**, 060505(R) (2009).
- [11] S. Wu and K. V. Samokhin, Effects of interface spin-orbit coupling on tunneling between normal metal and chiral p -wave superconductor, *Phys. Rev. B* **81**, 214506 (2010).
- [12] S. Kashiwaya, H. Kashiwaya, H. Kambara, T. Furuta, H. Yaguchi, Y. Tanaka, and Y. Maeno, Edge states of Sr_2RuO_4 detected by in-plane tunneling spectroscopy, *Phys. Rev. Lett.* **107**, 077003 (2011).
- [13] M. Anwar, S. Lee, R. Ishiguro, Y. Sugimoto, Y. Tano, S. Kang, Y. Shin, S. Yonezawa, D. Manske, H. Takayanagi, T. W. Noh, and Y. Maeno, Direct penetration of spin-triplet superconductivity into a ferromagnet in $\text{Au}/\text{SrRuO}_3/\text{Sr}_2\text{RuO}_4$ junctions, *Nat. Commun.* **7**, 13220 (2016).
- [14] L. A. B. Olde Olthof, S.-I. Suzuki, A. A. Golubov, M. Kunieda, S. Yonezawa, Y. Maeno, and Y. Tanaka, Theory of tunneling spectroscopy of normal metal/ferromagnet/spin-triplet superconductor junctions, *Phys. Rev. B* **98**, 014508 (2018).
- [15] K. Ishida, H. Mukuda, Y. Kitaoka, K. Asayama, Z. Q. Mao, Y. Mori, and Y. Maeno, Spin-triplet superconductivity in Sr_2RuO_4 identified by ^{17}O knight shift, *Nature* **396**, 658 (1998).
- [16] T. M. Rice and M. Sigrist, An electronic analogue of $3he^?$, *J. Phys.: Condens. Matter* **7**, L643 (1995).
- [17] T. Nomura and K. Yamada, Perturbation theory of spin-triplet superconductivity for Sr_2RuO_4 , *J. Phys. Soc. Jpn.* **69**, 3678 (2000).
- [18] M. Sato and M. Kohmoto, Mechanism of spin-triplet superconductivity in Sr_2RuO_4 , *J. Phys. Soc. Jpn.* **69**, 3505 (2000).
- [19] T. Takimoto, Orbital fluctuation-induced triplet superconductivity: Mechanism of superconductivity in Sr_2RuO_4 , *Phys. Rev. B* **62**, R14641 (2000).
- [20] K. Kuroki, M. Ogata, R. Arita, and H. Aoki, Crib-shaped triplet-pairing gap function for an orthogonal pair of quasi-one-dimensional fermi surfaces in Sr_2RuO_4 , *Phys. Rev. B* **63**, 060506 (2001).
- [21] T. Nomura and K. Yamada, Detailed investigation of gap structure and specific heat in the p -wave superconductor Sr_2RuO_4 , *J. Phys. Soc. Jpn.* **71**, 404 (2002).
- [22] T. Nomura and K. Yamada, Roles of electron correlations in the spin-triplet superconductivity of Sr_2RuO_4 , *J. Phys. Soc. Jpn.* **71**, 1993 (2002).
- [23] Y. Yanase and M. Ogata, Microscopic identification of the d -vector in triplet superconductor Sr_2RuO_4 , *J. Phys. Soc. Jpn.* **72**, 673 (2003).
- [24] T. Nomura and K. Yamada, Theory of transport properties in the p -wave superconducting state of Sr_2RuO_4 – a microscopic determination of the gap structure –, *J. Phys. Soc. Jpn.* **74**, 1818 (2005).
- [25] T. Nomura, D. S. Hirashima, and K. Yamada, Possible collective spin excitation in the spin-triplet superconducting state of Sr_2RuO_4 : Multi-band theory, *J. Phys. Soc. Jpn.* **77**, 024701 (2008).
- [26] S. Raghu, A. Kapitulnik, and S. A. Kivelson, Hidden quasi-one-dimensional superconductivity in Sr_2RuO_4 , *Phys. Rev. Lett.* **105**, 136401 (2010).
- [27] M. Tsuchiizu, Y. Yamakawa, S. Onari, Y. Ohno, and H. Kontani, Spin-triplet superconductivity in Sr_2RuO_4 due to orbital and spin fluctuations: Analyses by two-dimensional renormalization group theory and self-consistent vertex-correction method, *Phys. Rev. B* **91**, 155103 (2015).
- [28] L.-D. Zhang, W. Huang, F. Yang, and H. Yao, Superconducting pairing in Sr_2RuO_4 from weak to intermediate coupling, *Phys. Rev. B* **97**, 060510 (2018).
- [29] W.-S. Wang, C.-C. Zhang, F.-C. Zhang, and Q.-H. Wang, Theory of chiral p -wave superconductivity with near nodes for Sr_2RuO_4 , *Phys. Rev. Lett.* **122**, 027002 (2019).
- [30] Z. Wang, X. Wang, and C. Kallin, Spin-orbit coupling and spin-triplet pairing symmetry in Sr_2RuO_4 , *Phys. Rev. B* **101**, 064507 (2020).
- [31] A. Pustogow, Y. Luo, A. Chronister, Y.-S. Su, D. A. Sokolov, F. Jerzembeck, A. P. Mackenzie, C. W. Hicks, N. Kikugawa, S. Raghu, E. D. Bauer, and S. E. Brown, Constraints on the superconducting order parameter in Sr_2RuO_4 from oxygen-17 nuclear magnetic resonance, *Nature* **574**, 72 (2019).
- [32] K. Ishida, M. Manago, K. Kinjo, and Y. Maeno, Reduction of the ^{17}O knight shift in the superconducting state and the heat-up effect by nmr pulses on Sr_2RuO_4 , *J. Phys. Soc. Jpn.* **89**, 034712 (2020).
- [33] A. Chronister, A. Pustogow, N. Kikugawa, D. A. Sokolov, F. Jerzembeck, C. W. Hicks, A. P. Macken-

- zie, E. D. Bauer, and S. E. Brown, Evidence for even parity unconventional superconductivity in Sr_2RuO_4 , Proceedings of the National Academy of Sciences **118**, 10.1073/pnas.2025313118 (2021).
- [34] A. J. Leggett and Y. Liu, Symmetry properties of superconducting order parameter in Sr_2RuO_4 , Journal of Superconductivity and Novel Magnetism **34**, 1647 (2021).
- [35] S. Ghosh, A. Shekhter, F. Jerzembeck, N. Kikugawa, D. A. Sokolov, M. Brando, A. P. Mackenzie, C. W. Hicks, and B. J. Ramshaw, Thermodynamic evidence for a two-component superconducting order parameter in Sr_2RuO_4 , Nat. Phys. **17**, 199 (2021).
- [36] D. F. Agterberg, The symmetry of superconducting Sr_2RuO_4 , Nat. Phys. **17**, 169 (2021).
- [37] S. Benhabib, C. Lupien, I. Paul, L. Berges, M. Dion, M. Nardone, A. Zitouni, Z. Q. Mao, Y. Maeno, A. Georges, L. Taillefer, and C. Proust, Ultrasound evidence for a two-component superconducting order parameter in Sr_2RuO_4 , Nat. Phys. **17**, 194 (2021).
- [38] A. T. Rømer, D. D. Scherer, I. M. Eremin, P. J. Hirschfeld, and B. M. Andersen, Knight shift and leading superconducting instability from spin fluctuations in Sr_2RuO_4 , Phys. Rev. Lett. **123**, 247001 (2019).
- [39] S. A. Kivelson, A. C. Yuan, B. Ramshaw, and R. Thomale, A proposal for reconciling diverse experiments on the superconducting state in Sr_2RuO_4 , npj Quantum Materials **5**, 43 (2020).
- [40] R. Willa, M. Hecker, R. M. Fernandes, and J. Schmalian, Inhomogeneous time-reversal symmetry breaking in Sr_2RuO_4 , Phys. Rev. B **104**, 024511 (2021).
- [41] J. Clepkens, A. W. Lindquist, X. Liu, and H.-Y. Kee, Higher angular momentum pairings in interorbital shadowed-triplet superconductors: Application to Sr_2RuO_4 (2021), arXiv:2107.00047 [cond-mat.supr-con].
- [42] A. C. Yuan, E. Berg, and S. A. Kivelson, Strain-induced time reversal breaking and half quantum vortices near a putative superconducting tetracritical point in Sr_2RuO_4 , Phys. Rev. B **104**, 054518 (2021).
- [43] J. Clepkens, A. W. Lindquist, and H.-Y. Kee, Shadowed triplet pairings in Hund's metals with spin-orbit coupling, Phys. Rev. Research **3**, 013001 (2021).
- [44] A. T. Rømer, P. J. Hirschfeld, and B. M. Andersen, Superconducting state of Sr_2RuO_4 in the presence of longer-range coulomb interactions, Phys. Rev. B **104**, 064507 (2021).
- [45] H. G. Suh, H. Menke, P. M. R. Brydon, C. Timm, A. Ramires, and D. F. Agterberg, Stabilizing even-parity chiral superconductivity in Sr_2RuO_4 , Phys. Rev. Research **2**, 032023 (2020).
- [46] D. F. Agterberg, P. M. R. Brydon, and C. Timm, Bogoliubov fermi surfaces in superconductors with broken time-reversal symmetry, Phys. Rev. Lett. **118**, 127001 (2017).
- [47] P. M. R. Brydon, D. F. Agterberg, H. Menke, and C. Timm, Bogoliubov fermi surfaces: General theory, magnetic order, and topology, Phys. Rev. B **98**, 224509 (2018).
- [48] C. M. Puetter and H.-Y. Kee, Identifying spin-triplet pairing in spin-orbit coupled multi-band superconductors, EPL (Europhysics Letters) **98**, 27010 (2012).
- [49] A. Ramires and M. Sgrist, Superconducting order parameter of Sr_2RuO_4 : A microscopic perspective, Phys. Rev. B **100**, 104501 (2019).
- [50] W. Chen and J. An, Interorbital p - and d -wave pairings between $d_{xz/yz}$ and d_{xy} orbitals in Sr_2RuO_4 , Phys. Rev. B **102**, 094501 (2020).
- [51] V. Grinenko, D. Das, R. Gupta, B. Zinkl, N. Kikugawa, Y. Maeno, C. W. Hicks, H.-H. Klauss, M. Sgrist, and R. Khasanov, Unsplit superconducting and time reversal symmetry breaking transitions in Sr_2RuO_4 under hydrostatic pressure and disorder, Nat. Commun. **12**, 3920 (2021).
- [52] Y. Yu, A. K. C. Cheung, S. Raghu, and D. F. Agterberg, Residual spin susceptibility in the spin-triplet orbital-singlet model, Phys. Rev. B **98**, 184507 (2018).
- [53] A. W. Lindquist and H.-Y. Kee, Distinct reduction of knight shift in superconducting state of Sr_2RuO_4 under uniaxial strain, Phys. Rev. Research **2**, 032055 (2020).
- [54] T. Scaffidi, J. C. Romers, and S. H. Simon, Pairing symmetry and dominant band in Sr_2RuO_4 , Phys. Rev. B **89**, 220510 (2014).
- [55] A. Ramires and M. Sgrist, Identifying detrimental effects for multiorbital superconductivity: Application to Sr_2RuO_4 , Phys. Rev. B **94**, 104501 (2016).
- [56] M. W. Haverkort, I. S. Elfimov, L. H. Tjeng, G. A. Sawatzky, and A. Damascelli, Strong spin-orbit coupling effects on the fermi surface of Sr_2RuO_4 and Sr_2RhO_4 , Phys. Rev. Lett. **101**, 026406 (2008).
- [57] C. N. Veenstra, Z.-H. Zhu, M. Raichle, B. M. Ludbrook, A. Nicolaou, B. Slomski, G. Landolt, S. Kittaka, Y. Maeno, J. H. Dil, I. S. Elfimov, M. W. Haverkort, and A. Damascelli, Spin-orbital entanglement and the breakdown of singlets and triplets in Sr_2RuO_4 revealed by spin- and angle-resolved photoemission spectroscopy, Phys. Rev. Lett. **112**, 127002 (2014).
- [58] H. S. Røising, T. Scaffidi, F. Flicker, G. F. Lange, and S. H. Simon, Superconducting order of Sr_2RuO_4 from a three-dimensional microscopic model, Phys. Rev. Research **1**, 033108 (2019).
- [59] V. L. Berezinskii, New model of the anisotropy phase of superfluid He^3 , JETP Lett. **20**, 287 (1974).
- [60] A. Balatsky and E. Abrahams, New class of singlet superconductors which break the time reversal and parity, Phys. Rev. B **45**, 13125 (1992).
- [61] K. Shigeta, S. Onari, K. Yada, and Y. Tanaka, Theory of odd-frequency pairings on a quasi-one-dimensional lattice in the hubbard model, Phys. Rev. B **79**, 174507 (2009).
- [62] Y. Tanaka, M. Sato, and N. Nagaosa, Symmetry and topology in superconductors –odd-frequency pairing and edge states–, J. Phys. Soc. Jpn. **81**, 011013 (2012).
- [63] J. Linder and A. Balatsky, Odd-frequency superconductivity, Rev. Mod. Phys. **91**, 045005 (2019).
- [64] D. S. Hirashima, Dynamical spin susceptibilities in the superconducting phase of Sr_2RuO_4 , J. Phys. Soc. Jpn. **76**, 034701 (2007).
- [65] D. Maruyama, M. Sgrist, and Y. Yanase, Locally non-centrosymmetric superconductivity in multilayer systems, J. Phys. Soc. Jpn. **81**, 034702 (2012).
- [66] T. Hashimoto, K. Yada, A. Yamakage, M. Sato, and Y. Tanaka, Bulk electronic state of superconducting topological insulator, J. Phys. Soc. Jpn. **82**, 044704 (2013).
- [67] S. Kashiwaya, Y. Tanaka, N. Yoshida, and M. R. Beasley, Spin current in ferromagnet-insulator-superconductor junctions, Phys. Rev. B **60**, 3572 (1999).
- [68] T. Hirai, Y. Tanaka, N. Yoshida, Y. Asano, J. Inoue, and S. Kashiwaya, Temperature dependence of spin-polarized transport in ferromagnet/unconventional superconduc-

- tor junctions, Phys. Rev. B **67**, 174501 (2003).
- [69] Y. Tanaka and S. Kashiwaya, Theory of tunneling spectroscopy of *d*-wave superconductors, Phys. Rev. Lett. **74**, 3451 (1995).
- [70] S. Kashiwaya and Y. Tanaka, Tunnelling effects on surface bound states in unconventional superconductors, Rep. Prog. Phys. **63**, 1641 (2000).